Effects of sorption and desorption of CO2 on the thermomechanical experimental behavior of HNBR and FKM O-rings - Influence of nanofiller-reinforced rubber

E. Lainé, J.-C. Grandidier, G. Benoit, B. Omnes, F. Destaing

Effects of sorption and desorption of CO_2 on the thermomechanical experimental behavior of HNBR and FKM O-rings - Influence of nanofiller-reinforced rubber

E. Lainé[1*], J.C. Grandidier[1], G. Benoit[1], B. Omnès[2] & F. Destaing[2]

[1]*Institut Pprime, CNRS, ISAE-ENSMA, Université de Poitiers, F-86962 Futuroscope, France*
[2]*Centre Technique des Industries Mécaniques, F-44308 Nantes Cedex 3, France.*

*Corresponding author:
Eric Lainé
eric.laine@ensma.fr

ABSTRACT: Despite its importance in sealing, a fundamental understanding of the behavior of elastomeric O-rings in a gas environment is still incomplete. Further experimental research is needed to obtain a precise predictive model which can describe the combined effects of gases and mechanical loading. The effect of CO_2 pressure (2, 4 and 6MPa) on the mechanical compression behavior of HNBR and FKM seals at two temperatures (60 and 130°C) is described in the paper. To evaluate the contribution of nanofiller reinforcement, experimental tests were carried out on two kinds of rubber which are reinforced or not with nanofiller (10 phr of expanded graphite). A ranking of materials was performed thanks to experimental database. HNBR seems to be the better candidate in the service conditions applied. Furthermore, the nanofillers which are introduced in the rubber can lead some damages in Rapid Gas Decompression conditions, notably when the zero pressure was applied (desorption).

Keywords: Elastomer, CO_2 pressure, mechanical tests, O-rings, identification, constitutive equation

1 INTRODUCTION

Carbon dioxide is a natural gas which is frequently encountered in hydrocarbon environments. Relatively low concentrations of CO_2 in hydrocarbon mixtures can cause significant swelling of the seal. More significantly, the effect of absorbed CO_2 upon rapid gas decompression (RGD) can be catastrophic if consideration is not given to the choice of polymer, cure, and particle reinforcement.

Hydrogenated nitrile butadiene rubber (HNBR) and fluorocarbon rubber (FKM) are well known for their resistance to chemical and thermal degradation [1-3]. Nonetheless, performance and functional life of polymer materials can be significantly affected when submitted to gas environment. Indeed, saturation conditions, especially in CO_2, are known to alter the gas permeability due to plasticizing effects in almost all polymers and this effect is more pronounced for elastomer components [4-7]. In addition, they are specially designed for resistance to RGD.

Recently, Haroonabadi et al [8] have shown that the thermal ageing (7 days at 100°C) of NBR vulcanizates depends strongly on crosslink density and mechanical properties. Thermal ageing of nitrile rubber samples increased crosslink density and decreased tensile and tear strength, resulting in a decrease in RGD resistance. Chen et al. [9] studied CO_2 diffusivity and solubility, and RGD resistance of HNBR and fluoroelastomer (FKM) elastomers containing carbon nanotubes. While the addition of carbon nanotubes may lead to an increase in mechanical properties, they have shown that it reduces the CO_2 diffusivity and solubility and therefore improves the RGD resistance of the reinforced elastomers.

However, a fundamental understanding of the behavior of elastomeric seals in a gas environment is necessary because it is still incomplete and more particularly on coupling effects (diffuso-mechanical). The lack of data in the literature comes from the difficulty of carrying out mechanical

tests to characterize the behavior under gaseous environment with a high gas pressure. Studies of the swelling behavior of elastomers under CO_2 are the most common in literature [10]. However, it should be noted that Davies et al. [7] have developed a standard dumbbell tensiometer to measure the mechanical properties of elastomers saturated with CO_2 and N_2 (two gases with very different solubilities) at pressures up to 4 MPa. High-pressure vessels installed on traction machines can be used, but carrying out such tests is not easy due to very restricted metrology. If it is relatively easy to measure the applied load or the actuator displacement, understand the local deformation is not obvious and requires specific equipment and tools. In addition to these difficulties, questions about the representativeness of the microstructure of the samples are generally considered, elastomer blocks are generally envisaged but their curing conditions are not identical to those of the seals. As a result, extrapolate behavior can lead to hazardous approximations.

The aim of this article is to propose a methodology coupling mechanical tests under extreme conditions (temperature and CO_2 pressure) with a local deformation measurement in order to identify the behavior of different elastomers. In addition, this method permits the characterization of the materials used in the structure (O-ring) obtained with the industrial process. In order to improve the measurements of the local strain, an in situ optical measuring system is used. This article focuses the study on HNBR and FKM respectively non-reinforced and reinforced with nanofillers in order to evaluate the matrices (HNBR, FKM) and the influence of these reinforcements on mechanical characteristics. Mechanical compression tests [11] were carried out on O-rings under CO_2 pressure (2, 4 and 6MPa) at two temperatures (60 and 130°C) and after CO_2 desorption. The selected CO_2 pressure and temperature values are in accordance with both NACE [12] and NORSOK M710 [13] standards. By comparing the different mechanical responses in the different configurations (temperature and CO_2 pressure), this procedure will evaluate the behavior and durability of each material. Ultimately, the parameters of the behavior law are modified and are a function of the temperature and CO_2 pressure.

2 EXPERIMENTAL

2.1 Materials and sample

Two elastomer types, a hydrogenated nitrile rubber (HNBR) and a fluorelastomer type (FKM) were selected for these investigations. The compounds were produced with a nominal hardness of 80 and 90 Shore A respectively for the HNBR and the FKM. HNBR and FKM were compounded as summarized in Table 1, respectively, using a base polymer which is 96% saturated with 36% acrylonitrile content and a 70% fluorine content. HNBR and FKM were vulcanized with peroxide curing systems, respectively dicumyl peroxide and DBPH.

The rubber matrices were reinforced with carbon black and nanofillers. The carbon black reinforcement is fixed at 100 phr. Both matrices were reinforced with 10 phr of nanofillers. The nanofiller chosen was expanded graphite with the reference TIMCAL (Timrex). The chosen denomination is 10GE for each rubber.

The compound of rubber was obtained with a "classical" compounding operating mode for an elastomer. An internal mixer was used to incorporate the nanofiller. Nanofillers were introduced before carbon black. To improve the homogenization of the compound and avoid delamination defect after curing, for FKM reinforced with nanofillers, two specific processing assistants were used. For HNBR, the incorporation of nanofillers reduces tensile strength and elongation at break. For FKM, the incorporation of nanofillers increases the loss factor for high strains.

Mechanical tests are not carried out on conventional specimens but directly on the industrial structure: O-ring. The nominal dimensional characteristics of the O-rings are 50.17mm x 5.33mm, respectively in terms of inner diameter and cross-section diameter.

Table 1. Composition of the HNBR and FKM assessed in the paper.

Materials	HNBR phr*	FKM phr*
NBR / FKM	100	100
N-330 HAF carbon black	70	20
Antioxydant agent	1.5	1.5
Vulcanisation agent		8
Vulcanizing agent	8	2.5
Vulcanizing accelerator	2	3
	+Nanofiller	+Nanofiller

* Parts per hundred rubber parts in weight.

2.2 Experimental device

An Instron 8802 servohydraulic fatigue machine (Figure 1a) was fitted with a pressure and temperature regulated chamber which allows mechanical testing in gaseous nitrogen, hydrogen or carbon dioxide up to 40MPa and 150°C. For safety reason related to hydrogen, the volume of the chamber is rather small (1.77liter with a diameter of 150mm and length of 100mm). More information on this device can be found in previous papers [14-15]. To observe the specimen, the vessel has a front and a back optical access through a central cylindrical sapphire window of 40mm diameter.

The fatigue machine, with a maximum capacity of 20kN, can operate up to a frequency of 20Hz. Its maximum stroke is 25 mm (limitation to the dimensions of the lower water jacket). However, the height of the chamber limits the dimensions of the various assemblies and test pieces. The fatigue machine is provided with an external load cell and a pressurized column containing a pressure compensated internal load cell. The presence of the internal load cell allows direct measurement of the applied load without any sealing friction forces. The whole of this device is temperature controlled. This device, named HYCOMAT, combines a purely mechanical load to a load of gas, under nitrogen (N_2), hydrogen (H_2), or carbon dioxide (CO_2).

2.3 Specific assembly

A specific assembly to test the seals was dimensioned and manufactured, for compressive tests (Figure 1b). A load reversal system is used in accordance of the ball joint alignment system of the test rig. This inverter assembly consists of two rigid U-shaped structures. Thus, the sample is placed on the upper U connected to the fixed jaw and the lower U is connected to the movable jaw to apply the compression (Figure 1b and Figure 1c). The trays are drilled in the center in order to avoid overpressure on the inside diameter of the O-ring during the compression test. The tensile mounting has been dimensioned so as to have at most one stroke a deformation in the seal of the order of 25%. The compression tests were limited to a 1.5mm crushing of the seal since this is equivalent to a local strain of the order of 25% in the section thereof. In practice, this type of seal in operation is compressed by a maximum of 15 to 25%.

Figure 1. a) global view and (b) magnification of the pressure CO_2 chamber of the experimental testing machine. (c) Specific U-shaped mounting for seal compression

2.4 Non-contact extensometry (markers method)

From the point of view of metrology, a system of non-contact extensometry is used. This method of markers, developed within the laboratory, has the advantage of being usable in extreme conditions (very high temperatures, high pressures ...). Markers (2 or 4) are placed on the O-rings's generatrix (Figure 2). This generatrix corresponds to the parting line of the O-ring, it is represented by a dotted line in the Figure 2. It is to follow the displacements of the barycentres of the tasks in the plane of a couple of markers (Figure 2). From this measurement of the relative displacement between two markers, a "local deformation" is deduced which is called deviation **(dev)**.

$$dev\ (\%) = \frac{\Delta L}{L_0} = \left(\frac{\sqrt{\left(X_k^i - X_k^j\right)^2 + \left(Y_k^i - Y_k^j\right)^2} - \sqrt{\left(X_0^i - X_0^j\right)^2 + \left(Y_0^i - Y_0^j\right)^2}}{\sqrt{\left(X_0^i - X_0^j\right)^2 + \left(Y_0^i - Y_0^j\right)^2}} \right) \times 100 \quad (1)$$

With regard to the O-rings, two or four markers are placed. This marking makes it possible to have a measurement of the dimensional changes by taking them two by two. The camera is centered between markers 2 and 3 (Figure 2). Markers 1 and 4 are the most misaligned. Deviations along the generatrix (Figure 2) at the parting line are measured respectively between markers 1 and 4 and markers 2 and 3. The measurement of deviations between the nearest (2 and 3) and furthest (1 and 4) markers respectively allows the values to be framed and the quality of measurements to be assessed with these markers. The average of the two is used to characterize the behavior of the material.

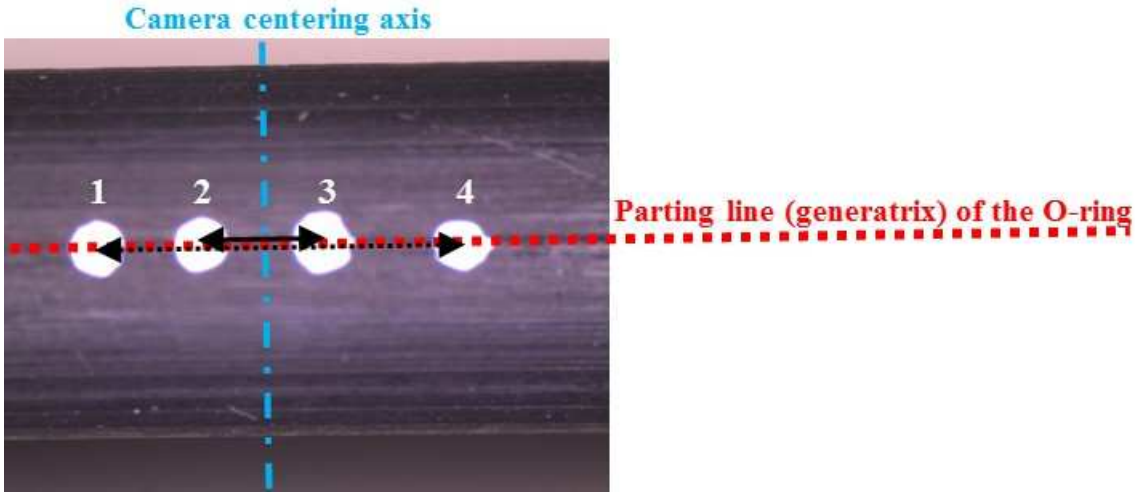

Figure 2 : Measurement deviations (dev 1-4 & 2-3) - complex markers Tracking Method

2.5 Protocol

The compression tests for each of the materials were carried out according to an identical protocol [11]. This one consists in several following steps:

- Step A: Positioning of the seal for compression test on the greased tray
- Step B: Temperature stabilization at 60 or 130°C (at least six hours).
- Step C: Compression tests at isothermal temperature (60 or 130°C).
- Step D: Pressurization under CO_2 (2,4 or 6MPa) at a speed between 2 and 4MPa/min, then stabilization for at least six hours (Figure 3a) in order to obtain the saturation.
- Step E: Compression tests at isothermal temperature (60 or 130°C) and constant CO_2 pressure.
- Step F: Back to a zero CO_2 pressure (Air) at a speed between 2 and 4MPa/min (Figure 3b), then stabilization for at least six hours in order to obtain the new level of saturation.
- Step G: Compression tests at isothermal temperature (60 or 130°C).

The pressurization under CO_2 of the chamber consists in injecting CO_2 into it initially filled with air at atmospheric pressure. Three pressures are imposed 2, 4 and 6MPa and at two temperatures. Thus, the actual pressure (partial pressure) in CO_2 can be calculated by considering the amount of CO_2 contained in the air with that added to reach the set pressure (2, 4 or 6MPa). In Table 2, the corresponding CO_2 partial pressure is given for each desired pressure. In the rest of the document, to simplify reading, only the desired pressures are indicated.

The CO_2 pressure and temperature values comply with both NACE [12] and NORSOK M710 [13] standards, and under NACE conditions the pressure is set at 5.2 MPa at room temperature. To study the impact of temperature and pressure on the diffusion effect (NORSOK M710), the values were gradually increased to 130°C and 6MPa. The temperature limit was imposed by the thermal resistance of the HNBR.

In addition, it should be noted that during these tests, the decompression rate (Figure 3b) is imposed by the machine. It is not possible to control this decompression rate.

Table 2. Equivalent imposed pressure - partial pressure of CO_2.

Imposed pressure of CO_2 (MPa)	2	4	6
Partial pressure of CO_2 (real) (MPa)	1.899	3.899	5.899

Before each mechanical test, load, displacement and deviation measurement are reset. The compression tests consist of loading up the specimen to reach the expected displacement value, and next the unloading step follow the same speed. Reproducibility tests were carried out to ensure the

feasibility of the optical measurements (Figure 4a-b) and to evaluate the quality of the measurements. The set of results presented below is the average of two or three tests for each configuration.

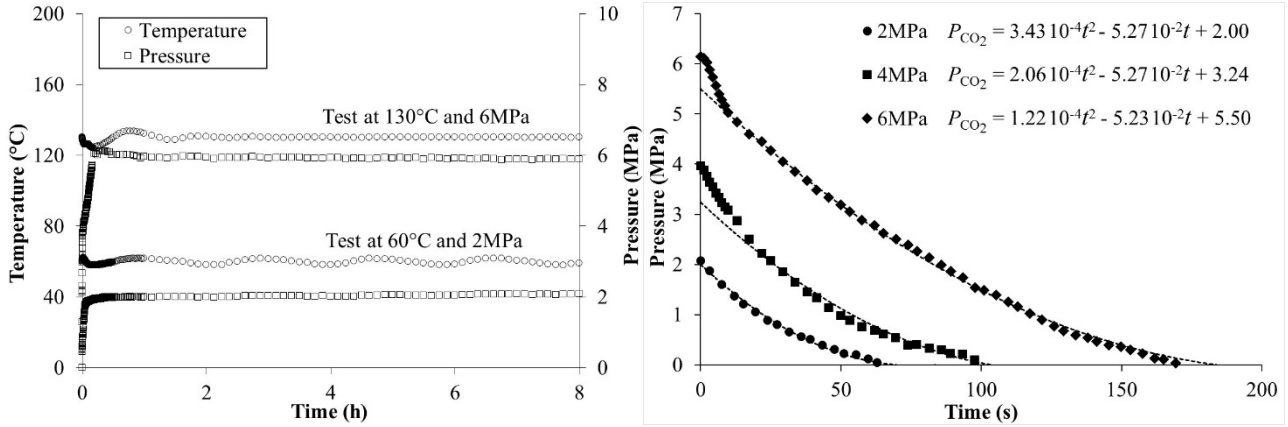

(a) (b)

Figure 3. (a) Time of stabilization – (b) Decompression rate, Pressure (P_{CO_2}) vs Time (t) [11]

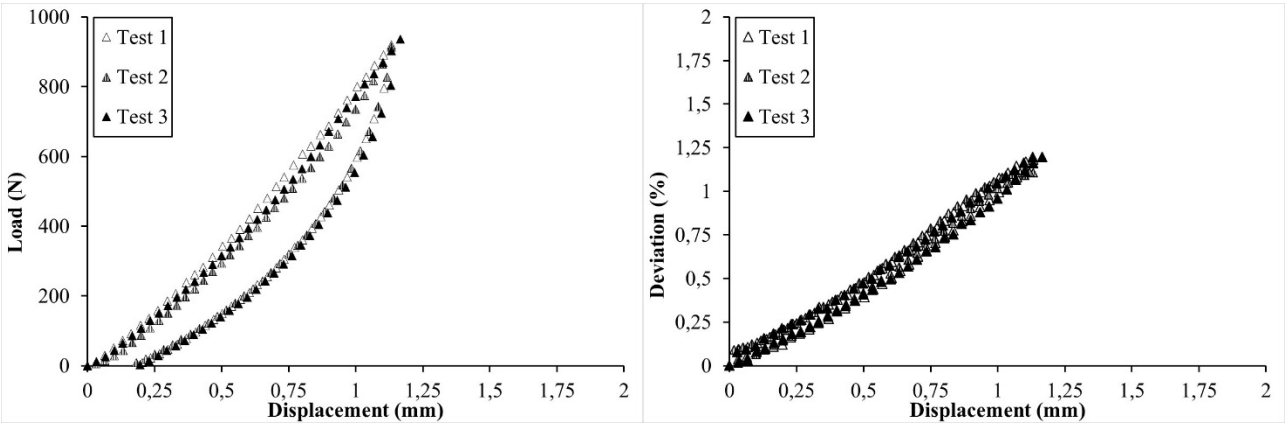

(a) (b)

Figure 4. Reproducibility of tests - compression test at 60°C for HNBR-10GE
(a) Load – Displacement curves, (b) Load – Deviation curves

3 FINITE ELEMENTS SIMULATIONS

3.1 Material Models

Seals with different materials (HNBR, FKM, HNBR-10GE, and FKM-10GE) are tested under uniaxial compression to establish load-displacement and deviation-displacement curves, so that an appropriate component model can be selected in the following finite element (FE) simulations. The tests were carried out around 25-30% compression, which corresponds to average deformations. To this end, a hyperelastic modeling model can be used to describe the behavior of elastomeric seals in our FE simulations. These simulations are performed using the commercial FEA (Finite Elements Analysis) software ABAQUS (User's Manual Version 6.13, Providence, RI, USA) [16].

To describe the behavior of the elastomers in this study, the neo-Hookean compressible form of the strain energy density function was chosen. Since only moderate strains are of concern in the current investigation. The strain energy density function W for a neo-Hookean compressible material is typically formed of the deviatoric and the volumetric terms [16-18] and expressed as:

$$W = C_{10}\,(I_1;^{-} - 3) + D_1\,(J - 1)^2 \qquad (2)$$

where C_{10} and D_1 are temperature-dependent material parameters representing the resistance to shear and the compressibility of the material respectively; $I_1;^{-}$ is the first deviatoric strain invariant defined as:

$$I_1;^{-} = \lambda_1;^{-2} + \lambda_2;^{-2} + \lambda_3;^{-2} \tag{3}$$

where the deviatoric stretches $\lambda_i;^{-} = J^{-1/3}\lambda_i$; J is the total volume ratio and λ_i are the principal stretches. The initial shear modulus and bulk modulus are given by:

$$\mu_0 = 2C_{10} \quad \text{and } K_0 = 2/D_1. \tag{4}$$

3.2 Finite elements compression models

Numerical simulations of a compression seal was used to evaluate the rigidity and compressibility of each material in different configurations (temperature, CO_2 pressure). For this purpose, a parametric study was carried out to know the influence of each parameter according to the test conditions. In addition, in relation to the measurement of the deviation, the numerical tool allows to evaluate, for example, the effect of a marker positioning error on the measurement. First, two models can be considered depending on the test conditions: 3D and axisymmetric. The responses of these two models in load and deviation were compared to determine the most relevant in terms of calculation time. The 3D geometric models in compression is defined in Figure 5a. This represents the seal as used and positioned in the chamber. Thermal and diffusion (CO_2) expansions are considered in the numerical model by adapting the initial geometry of the O-ring. Given the symmetry conditions, only a quarter of the O-ring is considered (Figure 5a), defined as a deformable solid. The compression plate and the lower support are represented by discrete rigid surfaces. The contact is managed between the different elements (seal and lower and upper plates) with a friction coefficient of 0.2 to ensure the stability of the numerical simulation. A parametric study of the friction coefficient showed that the compression response was independent of the friction coefficient in the observed deformation range. The finite elements used for the seal are C3D20H elements. The model is therefore represented by 8256 elements and 37645 nodes (Figure 5b). In the case of axisymmetric modeling (Figure 6), the rubber O-ring is meshed with eight node axisymmetric quadrilateral elements with hybrid formulation (CAX8H) accounting for the incompressibility of rubber materials. The model is composed of 2272 elements and 8485 nodes (Figure 6b).

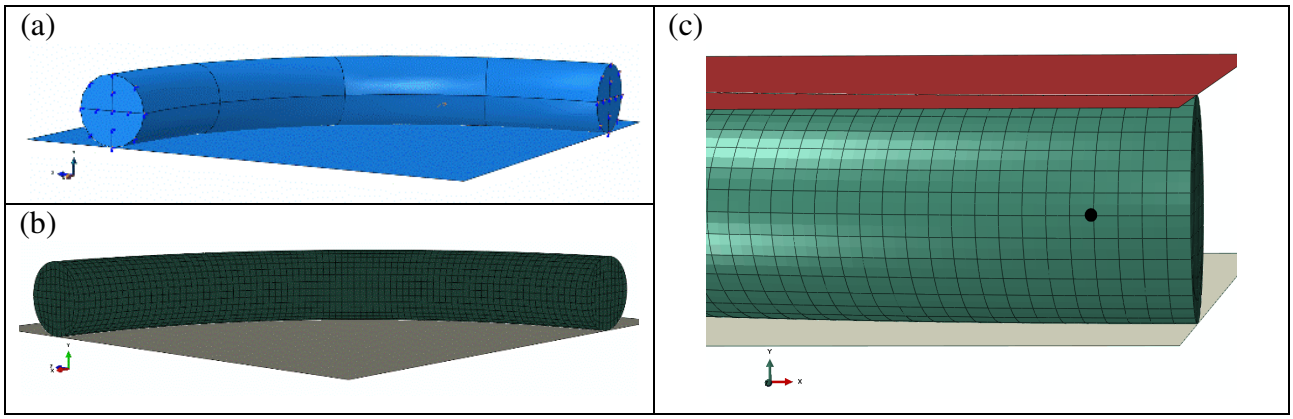

Figure 5 : 3D modeling of the quarter of the seal – Compression test (a) Geometry - (b) Mesh - (c) 3D Modeling - The black dots correspond to the nodes where the displacements are extracted to calculate the deviation in the cases

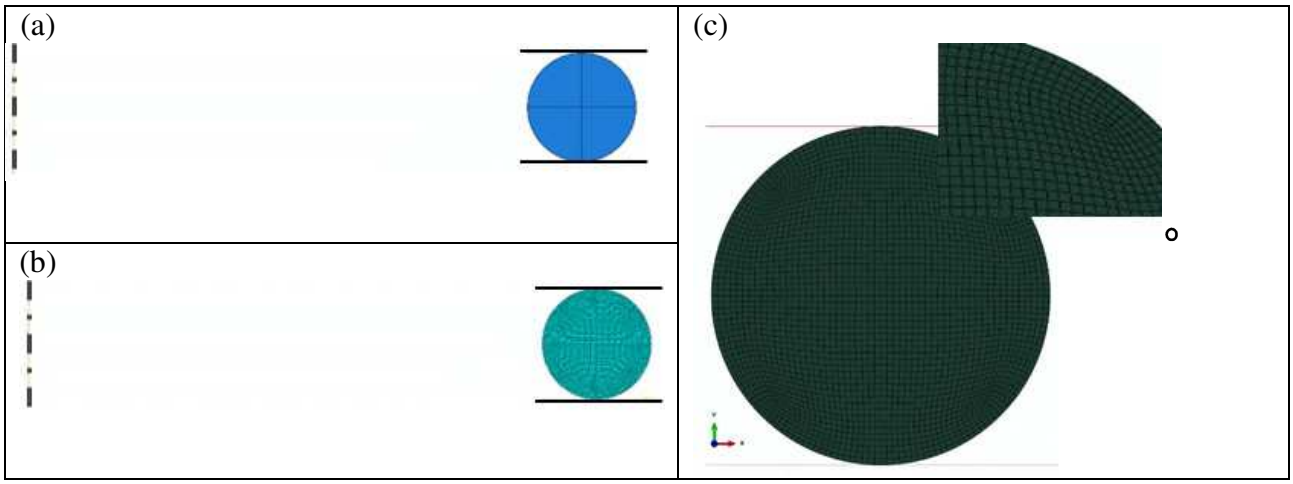

Figure 6 : Axisymmetric seal modeling – Compression test (a) Geometry - (b) Mesh - (c) 3D Modeling - The black dots correspond to the nodes where the displacements are extracted to calculate the deviation in the cases

3.2.1 Influence of modeling

First, the two models (3D and axisymmetric) are compared for different behaviors of generic elastomers in order to evaluate and compare the load and deviation responses. The behavior of the generic elastomer is given by the deformation energy density function (2) with C_{10}=1MPa, in the incompressible case and for two different compressibility values (D_1=0.1 and 0.2MPa^{-1}).

In 3D modeling, the deviation response is obtained by extracting the displacements of the nodes (Figure 5c) corresponding to the barycenter of the markers. Since only a quarter of the seal is represented thanks to the two symmetries, it is therefore assumed that the markers are perfectly symmetrical. Thus, it is enough to extract the coordinates of a single node. In the case of axisymmetric modeling, it is sufficient to also extract the coordinates of the node in the joint plane, external side of the seal (Figure 6c) and to project them in the perpendicular plane (XZ) in order to have the 3D coordinates of this node.

Figure 8 compares the different responses according to the two models and the laws of elastomer behavior. Figure 8a shows the load-displacement curves and Figure 8b shows the deviation-displacement curves. Whatever the behavior law and for average deformations (<25%), the two models give almost the same load-displacement responses. In the incompressible case the relation deviation-displacement are exactly the same. On the other hand, there is a slight difference between the two models for a deviation of more than 1.5%. However, the difference observed numerically is less than the accuracy of the measurement. Thus, it is quite possible to use the axisymmetric model to identify the parameters of the behavior law of an elastomer up to 25% strain.

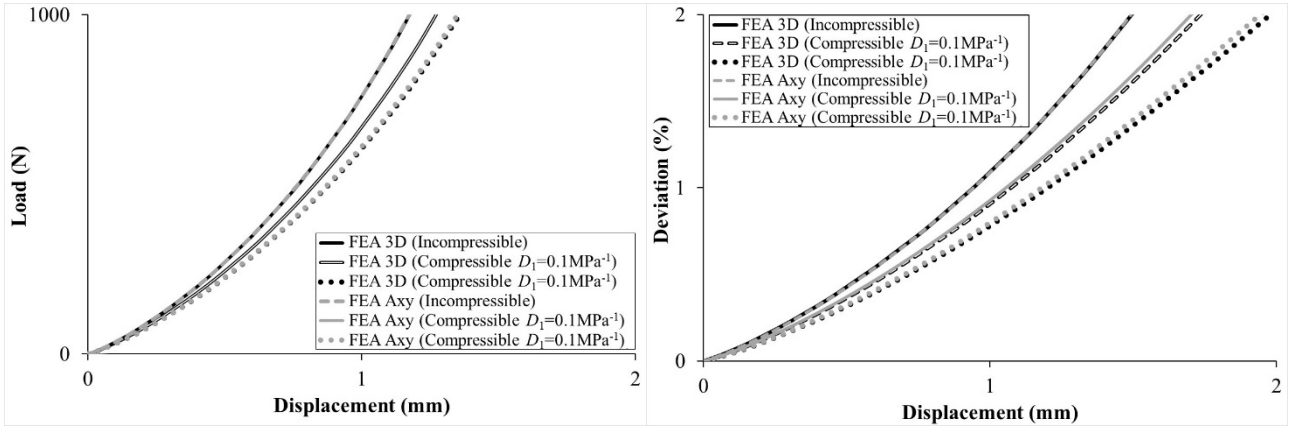

(a) (b)

Figure 7. Simulation answers for the compression test of an elastomeric seal (a) Load – Displacement curves (b) Deviation – Displacement curves

3.2.2 Influence of the parameters of the behavior law

First, a parametric study was conducted using the compression test simulation model. This study aims to evaluate the influence of the two parameters (C_{10} and D_1) of the behavior law (equation 2). Figure 8a, shows that the variation of the C_{10} coefficient, when D_1 is constant, has an important influence on the response in load. The loading is mainly compression, but the seal is free of shape, so only C_{10} participates in the stiffness since the volume change is not constrained. On the other hand, the evolution of the radius of the seal section is directly related to D_1. To illustrate this point, Figure 8b shows that the variation in the C_{10} coefficient, when D_1 is constant, is negligible on the deviation measurement. Conversely, if the coefficient D_1 varies and C_{10} is constant (Figure 9a and b) then the measurement of the deviation also varies. This confirms that the measurement of the deviation is only dependent on the compressibility coefficient D_1.

Moreover, Figure 9a and Figure 9b clearly show the dependence of the deviation on the coefficient D_1, since the curves on these last two figures shift in much the same way. On the other hand, in small deformations (<5%), the influence of parameter D_1 only starts at 0.1MPa^{-1} (which corresponds to a Poisson's ratio of 0.475) on the deviation measurement. Below this value, the measurements obtained during the tests can be considered to be within the measurement uncertainty.

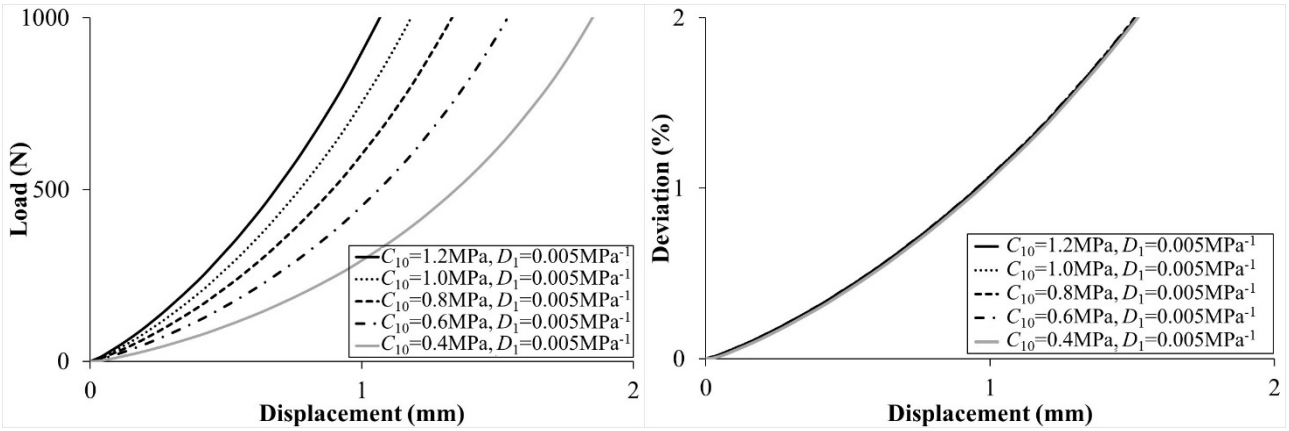

(a) (b)

Figure 8. Compression response - influence of behavior law parameter C_{10}

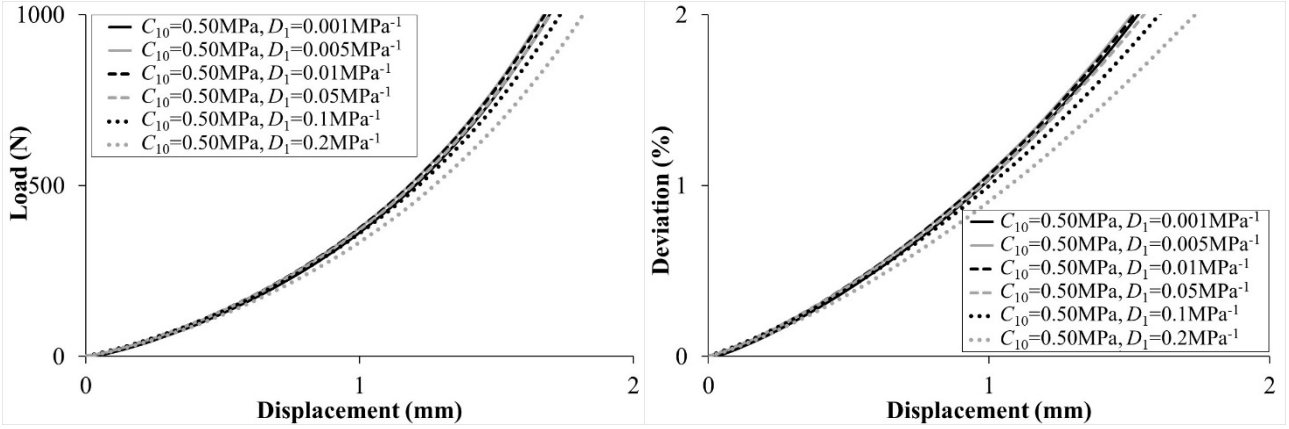

(a) (b)

Figure 9. Compression response - influence of behavior law parameter D_1

Figure 10a and b show that by measuring the three quantities (load, displacement and deviation) simultaneously during a compression test, there is only one solution of the parameter set (C_{10}, D_1).

Indeed, if figure 10b which represents the displacement deviation presents two almost superimposed curves for the parameter pairs C_{10}=1MPa, D_1=0.1MPa^{-1} and C_{10}=0.5MPa, D_1=0.2MPa^{-1}, Figure 10a representing the load as a function of displacement totally distinguishes these two responses.

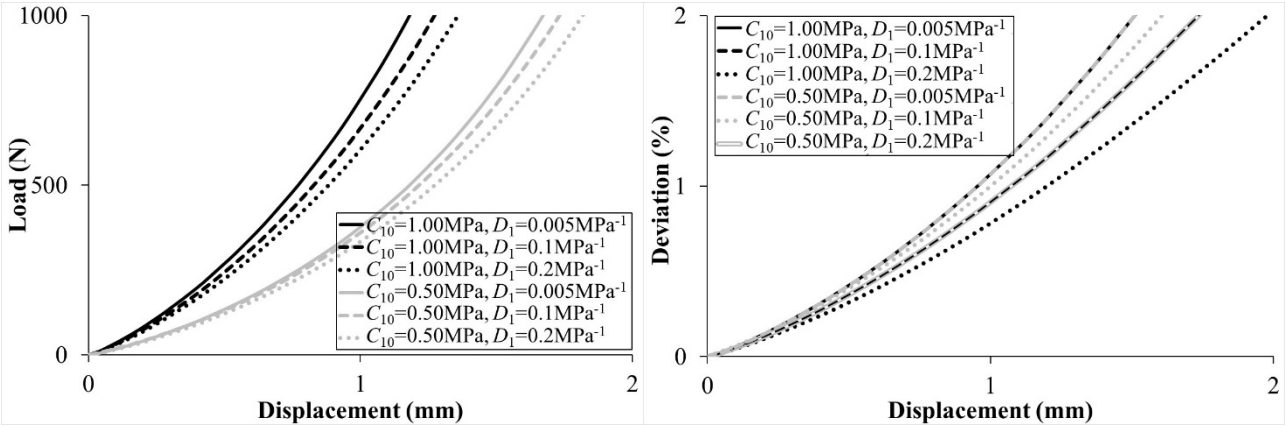

(a) (b)

Figure 10. Compression response for different stiffness values

Finally, from the compression tests on the seal, by simultaneously measuring the quantities: displacement of the compression plate and the load as well as the non-contact measurement of the swell (deflection), it is then possible to determine the set of parameters (C_{10}, D_1) of the behavior law (eq. 2) in small deformations.

4 RESULTS AND DISCUSSION

4.1 HNBR (Compression tests at 60°and 130°)

Compression tests on one HNBR seal at different CO_2 pressures (2, 4 and 6MPa) and at two temperatures (60 and 130°C) were performed on four different seals. The load-displacement curves and deviation-displacement are shown in Figures 11a and 11b at 60°C and 130°C respectively. The load-displacement curves at 60°C in Figure 11a show a slight loss of stiffness with increasing CO_2 pressure. The C_{10} coefficient decreases by almost 20% between the unsaturated material and the material subjected to a pressure of 6MPa in CO_2. The responses of HNBR without pressure (unsaturated) and at 2MPa are almost superimposed. However, the deviation-displacement curves at 60°C (Figure 11b) are all superimposed. This means that for HNBR, the effect of CO_2 pressure is zero or negligible on the compressibility of the material (D_1=0.075MPa^{-1}) up to about 25% deformation. In Figure 11b, the load-displacement curves at 4 and 6 MPa pressure at 130°C are very close to each other, and very slightly distinct from the unsaturated material. The deviation-displacement curves (figure 11b) are almost superimposed. The value of the compressibility coefficient is slightly higher for zero pressure than for the other two conditions (4 and 6MPa). Finally for HNBR, CO_2 sorption reduces the compression stiffness of the material between 0 and 6MPa, about 20% and 15% respectively at 60°C and 130°C. However, at both temperatures, it appears that the compressibility coefficient is the same and is not affected by CO_2.

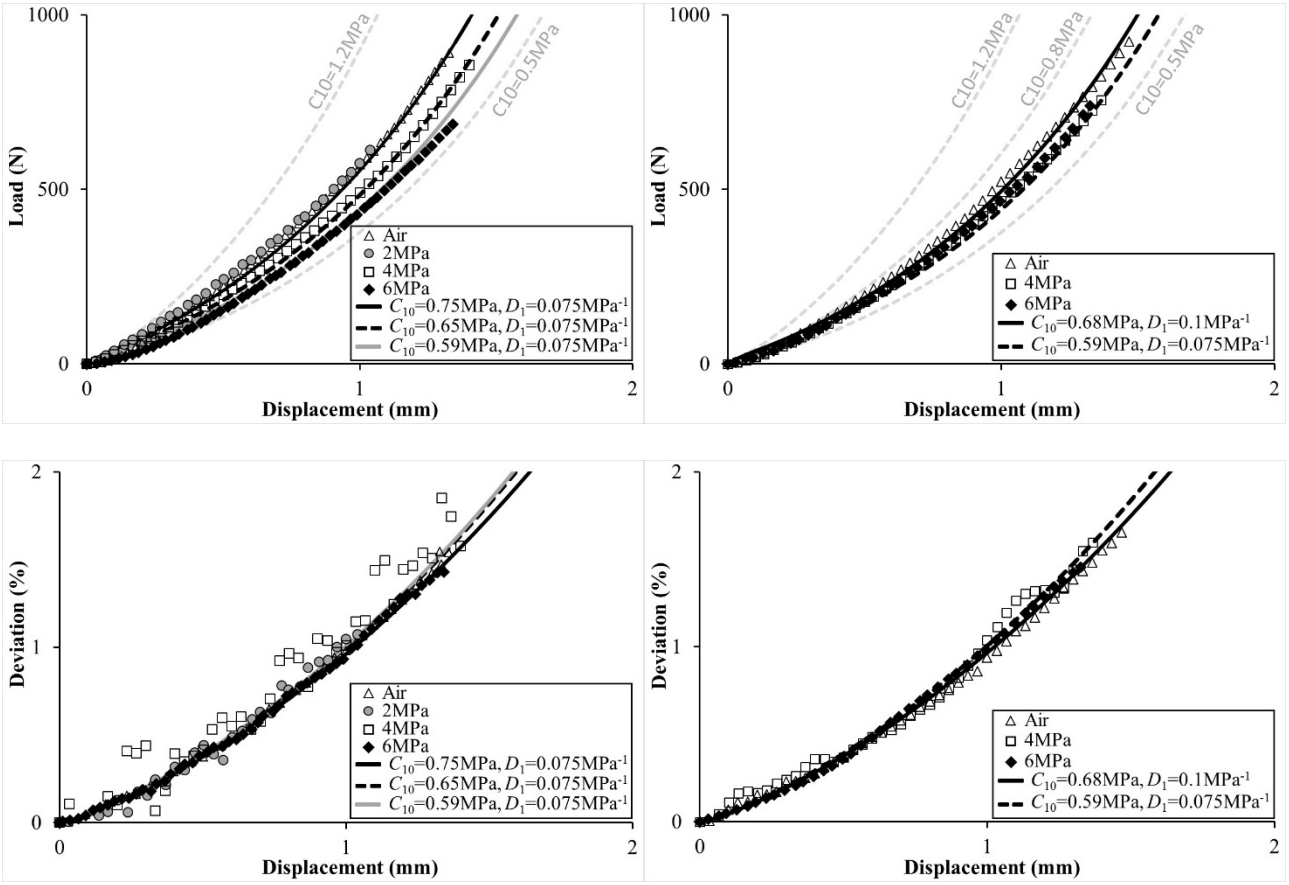

Figure 11. HNBR – Compression tests at (a) 60°C and (b) 130°C

4.2 FKM (Compression tests at 60°and 130°)

In the same manner compression tests on a FKM seal at different CO_2 pressures (2, 4 and 6MPa) and at two temperatures (60 and 130°C) were carried out on four different seals. The load - displacement curves are shown in Figure 12a and Figure 12b respectively at 60°C and 130°C. As for the HNBR, the CO_2 absorption at 60°C has an impact on the behavior of the FKM seal. Thus, the increase in the pressure of CO_2 causes a loss of the compression rigidity of the seal. It is higher in comparison with the HNBR. On the other hand, the conclusion between the two materials is not the same at 130°C, since there is a significant influence on the stiffness in compression and in particular on the response to 6MPa for the FKM seal. Note that to more accurately model the behavior of FKM under air at 130°C, for moderate strains (for a displacement greater than 1mm, Figure 12), it would be necessary to increase the number of parameters of the behavior law (Mooney-Rivlin or Polynomial Type).

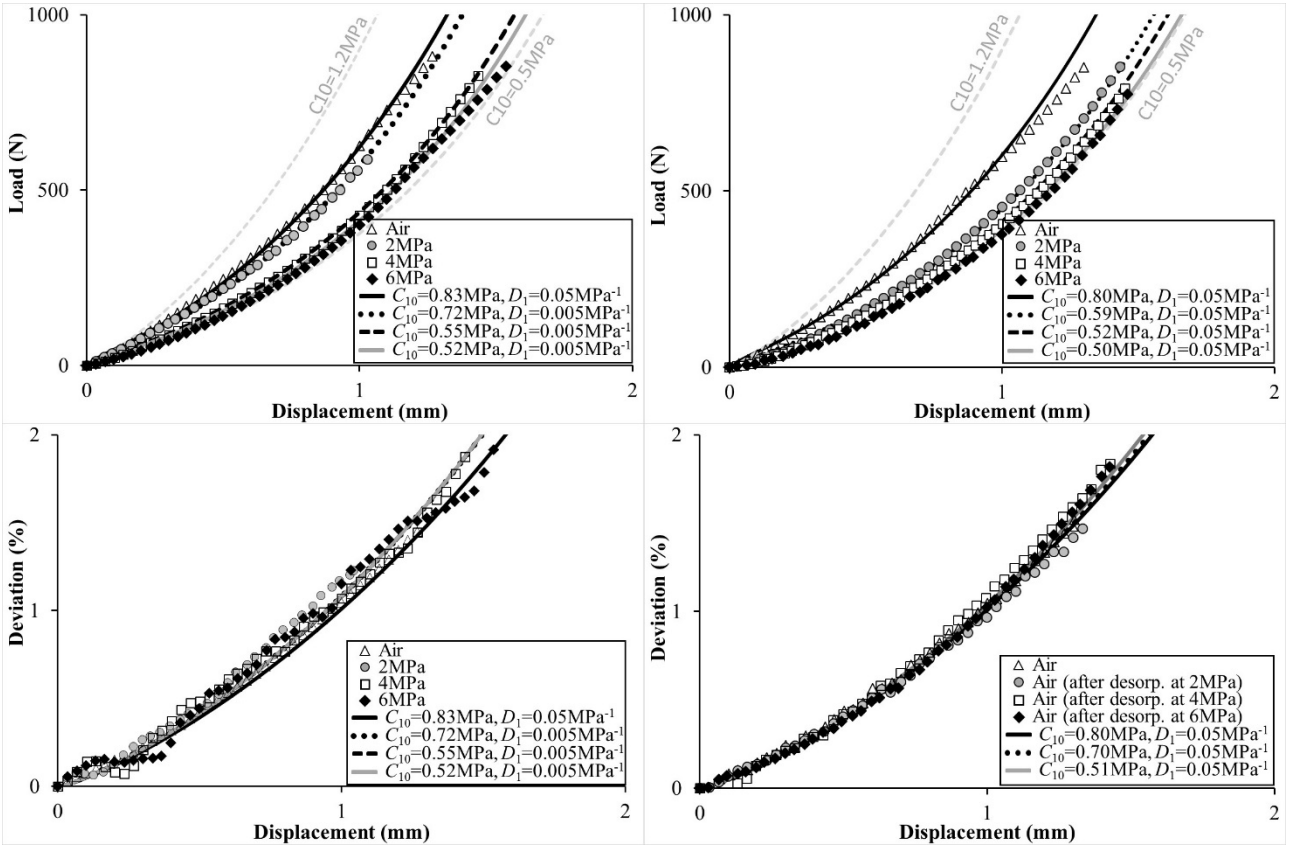

(a) (b)

Figure 12. FKM – Compression tests at (a) 60°C and (b) 130°C

4.3 Compression tests after CO_2 desorption (HNBR & FKM)

The final step of the test protocol (see 2.4) was to perform a compression test after total CO_2 desorption of the seal. The objective is to evaluate the impact of the pressure level applied at step D of the protocol on the final compression stiffness of the material.

Thus, a comparison between load-displacement and deviation-displacement responses is presented in Figure 13a and b respectively at 60 and 130°C. It can be seen on these figures that for the material HNBR, all the curves almost overlap. This indicates that imposing up to 6MPa CO_2 pressure on an HNBR seal has no effect on its mechanical characteristics (rigidity and compressibility). The seal suffers no damage and recovers its initial stiffness (C_{10}=0.75MPa at 60°C and 0.68MPa at 130°C) and compressibility (0.075MPa^{-1} at 60 and 130°C) at both temperatures. For the FKM seal it is also possible to measure a loss of rigidity generated by the history combining the mechanical loading and the gas pressure, this loss is of the same order of magnitude as that observed on the responses under pressure. The material retained the memory of the pressure phase (Figure 14a). On the other hand, the loss of rigidity is also observed at 130°C after an exposure to 4 and 6 MPa of CO_2. Thanks to the optical access, local swellings on the seal were observed during decompression. This swelling is the first demonstration of damage inside the materials (Figure 14b), the second is the loss of rigidity measured after exposure. Although this loss of stiffness is small, one can imagine that a succession of sorption/desorption at these pressures would lead to the rapid degradation of the FKM seal.

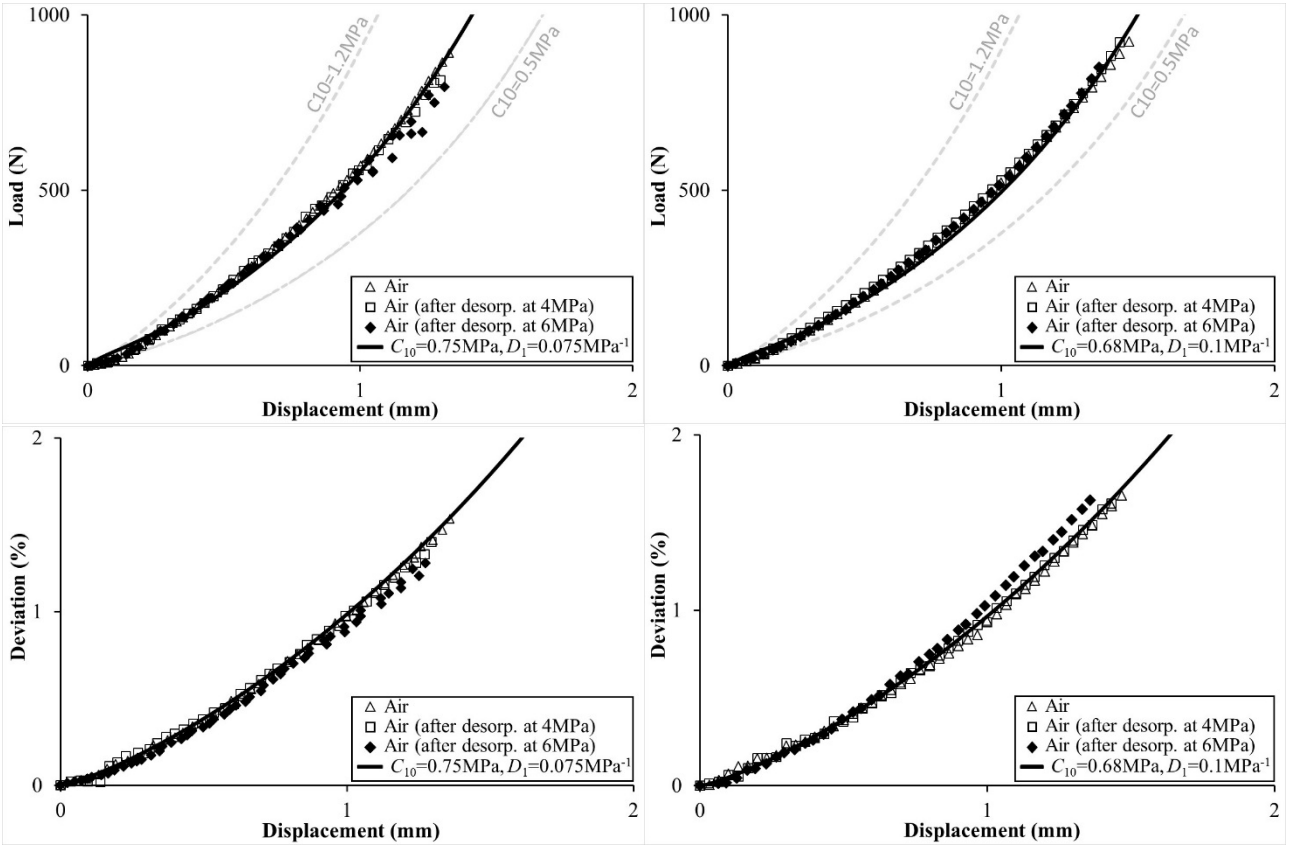

(a) (b)

Figure 13 HNBR - Compression tests under air at (a) 60°C and (b) 130°C after CO_2 desorption

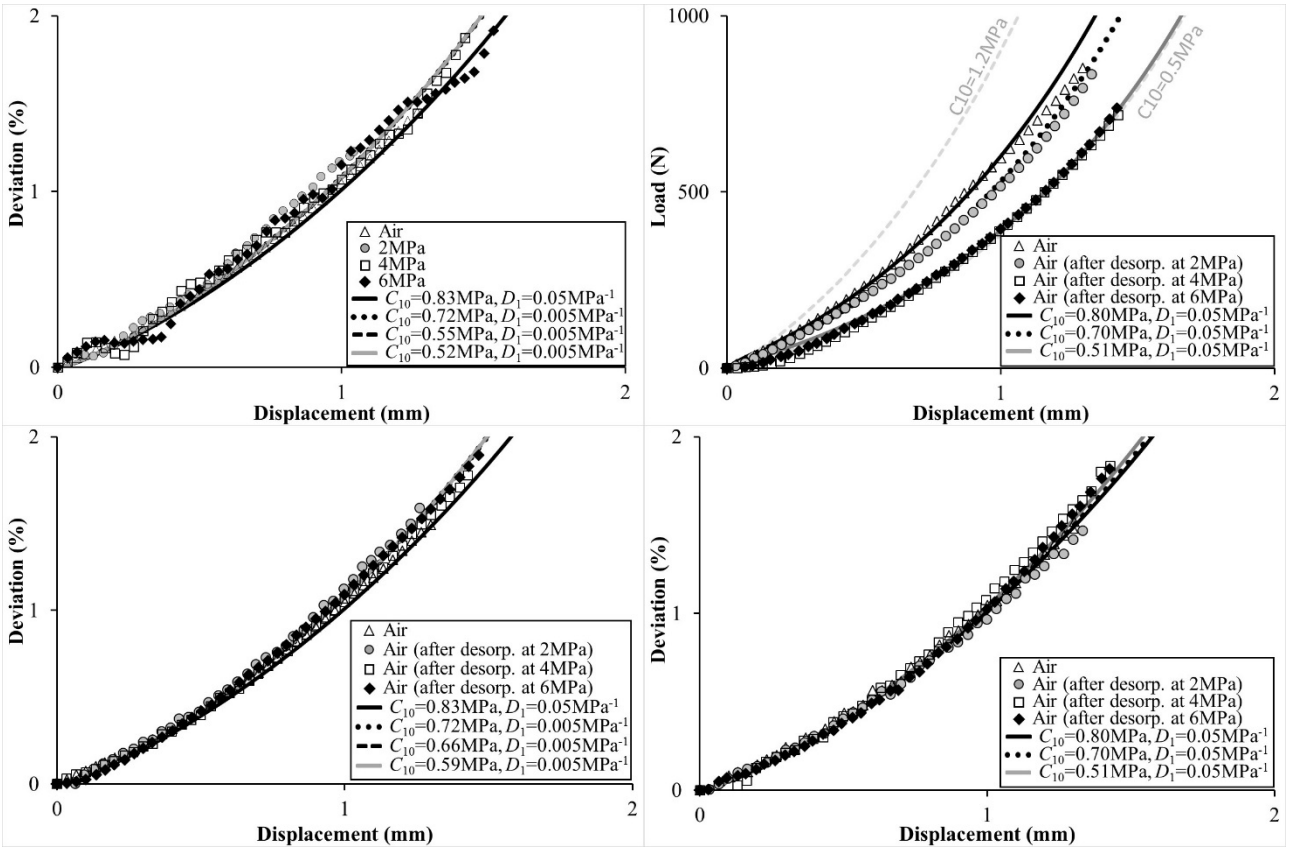

(a) (b)

Figure 14. FKM – Compression tests under air at (a) 60°C and (b) 130°C after CO_2 desorption

4.4 Effects of 10GE reinforcements on the HNBR matrix

Compression tests on a HNBR-10GE seal at different CO_2 pressures (2, 4 and 6MPa) and at two temperatures (60°C and 130°C) were carried out on four different O-rings. The load-displacement curves are shown in Figure 15a and Figure 15b respectively at 60°C and 130°C. The results of compression tests with return to zero pressure are presented on Figure 16a and Figure 16b.

For HNBR-10GE, it is noted in Figure 15a and Figure 15b the rigidity decreases progressively with the increase in CO_2 pressure. However, in a healthy state, this material is more rigid at 60°C than at 130°C. Note that to more accurately model the behavior of HNBR-10GE under air at 60°C, for moderate deformations (for a displacement greater than 1mm, Figure 15a), it would be necessary to increase the number of parameters of the behavior law (Mooney-Rivlin or Polynomial Type). However, when subjected to a pressure of 6MPa of CO_2, it gives almost the same response at both temperatures. Thus, the loss of rigidity is 46% and 22.5% respectively at 60 and 130°C. The compressibility coefficient of the HNBR-10GE is slightly lower than for the HNBR. That seems obvious from the charges. If the load-displacement curves of figures 15a and b show that the compressibility of healthy material (0MPa) is different at 60 and 130°C, they also show that the presence of CO_2 leads to a decrease in this coefficient and tends towards the incompressibility of the material. At 60°C, it can be considered that there is a transition, for a given pressure value between 2 and 4MPa, for which the compressibility of the HNBR-10GE changes.

The load-displacement curves of figures 16a (60°C) and b (130°C) show that after desorption of CO_2, only seals subjected to a CO_2 pressure of 2MPa regain the initial behavior. For the other two configurations (4 and 6MPa), the loss of stiffness is significant (30% for 6MPa). However, the displacement curves in Figures 16a (60°C) and b (130°C) show that sorption and CO_2 desorption have no effect on the compressibility of HNBR-10GE. The curve after desorption at 4MPa is not retained because it seems that a measurement problem appeared after 0.2mm of displacement of the plate.

Finally, the compressibility values obtained at 60°C, are relatively close (0.05 and 0.075MPa^{-1}) not to be distinguished. In addition, we found here the value identified for the HNBR seal at 60°C, which is not the case at 130°C. It is therefore obvious that, compared to the responses under the same conditions (temperature and pressure) with the HNBR matrix, this reinforced material degrades under the effect of CO_2 (pressure and / or desorption). Thus, the 10GE reinforcements render the matrix having been subjected to a certain CO_2 pressure (between 0 and 2 MPa) and a CO_2 desorption following the imposed speed.

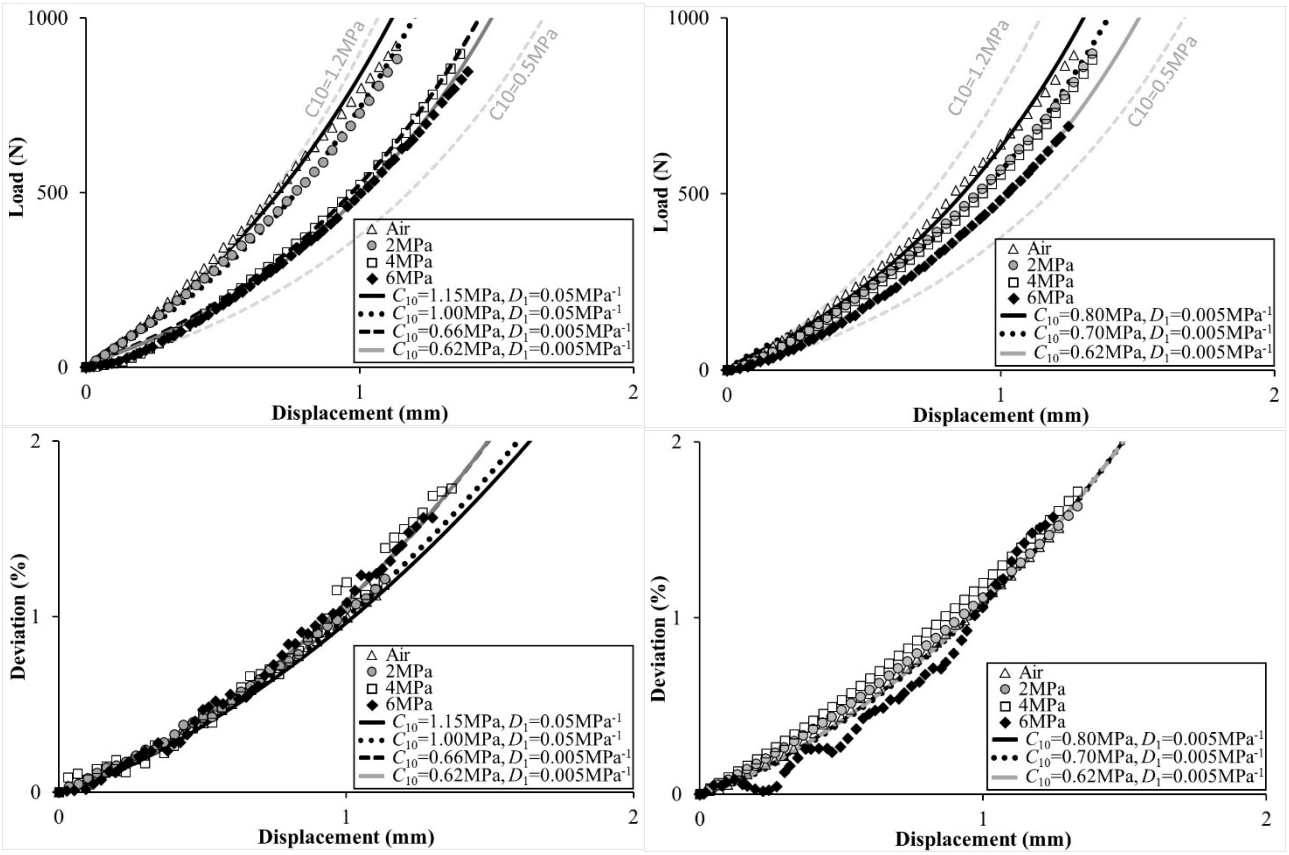

(a) (b)

Figure 15. HNBR-10GE – Compression tests at (a) 60°C and (b) 130°C

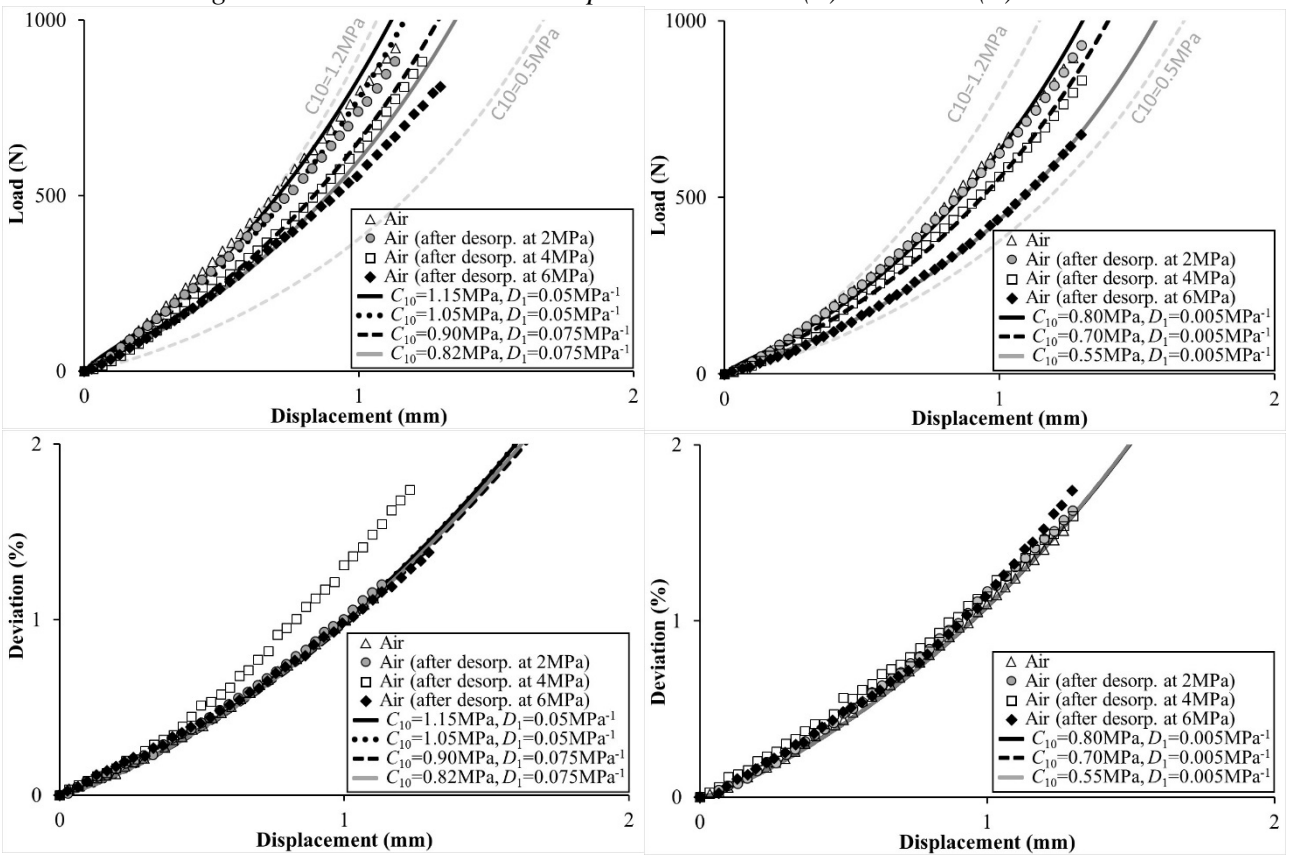

(a) (b)

Figure 16. HNBR-10GE – Compression tests under air at (a) 60°C and (b) 130°C after CO_2 desorption

4.5 Effects of 10GE reinforcements on the FKM matrix

Compression tests on a FKM-10GE seal at different CO_2 pressures (2, 4 and 6MPa) and at two temperatures (60°C and 130°C) were carried out on four different O-rings. The load - displacement curves and deviation – displacement are shown in Figure 17a and Figure 17b respectively at 60°C and 130°C. The results of compression tests with return to zero pressure are presented on Figure 18a and Figure 18b.

For FKM-10GE, it is noted in Figure 17a and Figure 17b the rigidity decreases progressively with the increase in CO_2 pressure as for other materials. However, in a healthy state, this material is more rigid at 60°C than at 130°C. It can be seen in Figure 17a that its behavior at 60°C is more sensitive to CO_2 pressure than at 130°C (Figure 17b), because its rigidity decreases significantly with increasing CO_2 pressure. Under a pressure of 6MPa in CO_2, the decrease in rigidity is nearly 40% at 60°C compared to 24% at 130°C. In addition, at both temperatures, the coefficient of compressibility tends to increase with increasing pressure.

The compression tests after desorption of CO_2 clearly show that this reinforced material (FKM-10GE) is strongly damaged. Indeed, its residual rigidity is reduced from the 2 MPa exposition at 60°C (Figure 18a) and the 4 MPa exposition at 130°C (Figure 18b). This damage can be generated by the load applied under pressure but it can be also initiated during the CO_2 desorption, but in any case it depends on the initial pressure.

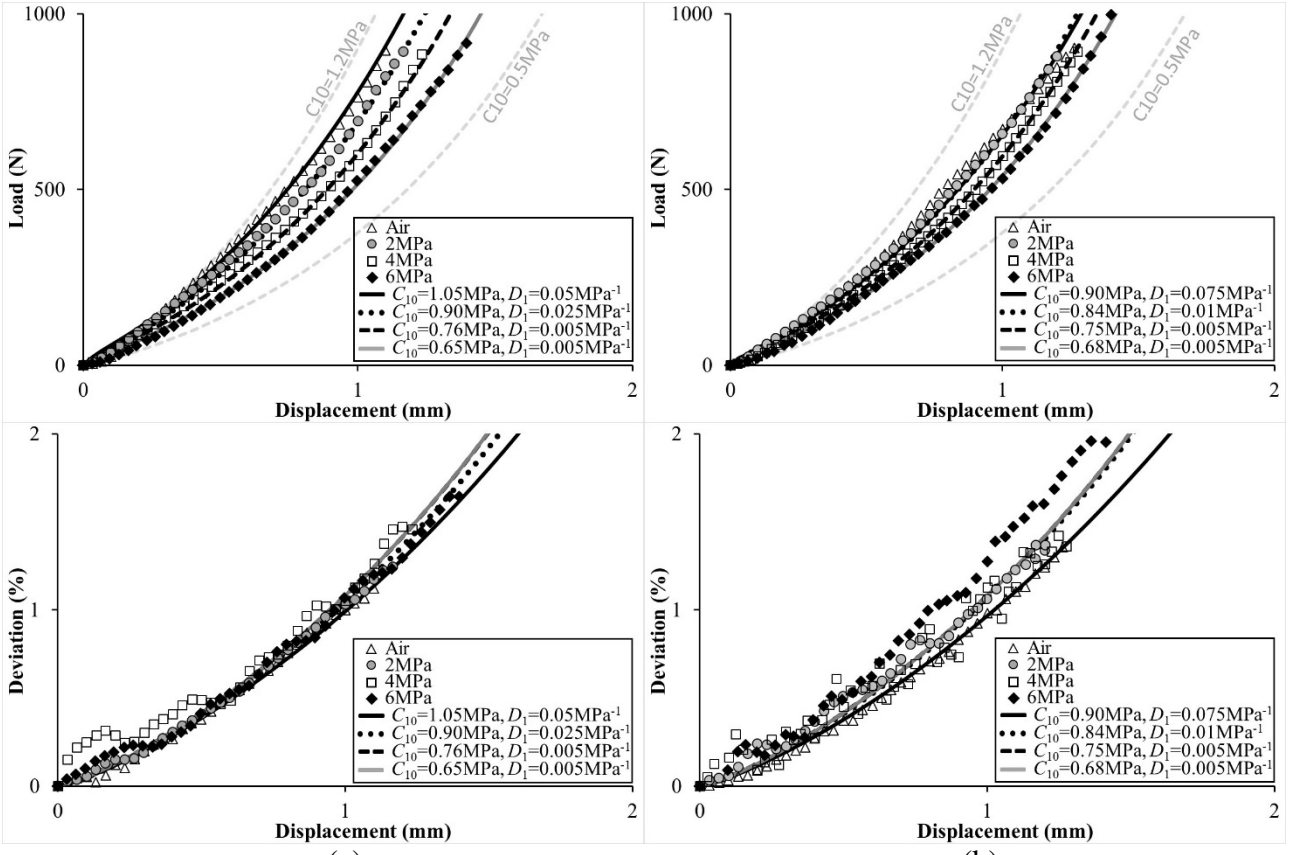

Figure 17. FKM-10GE – Compression tests at (a) 60°C and (b) 130°C

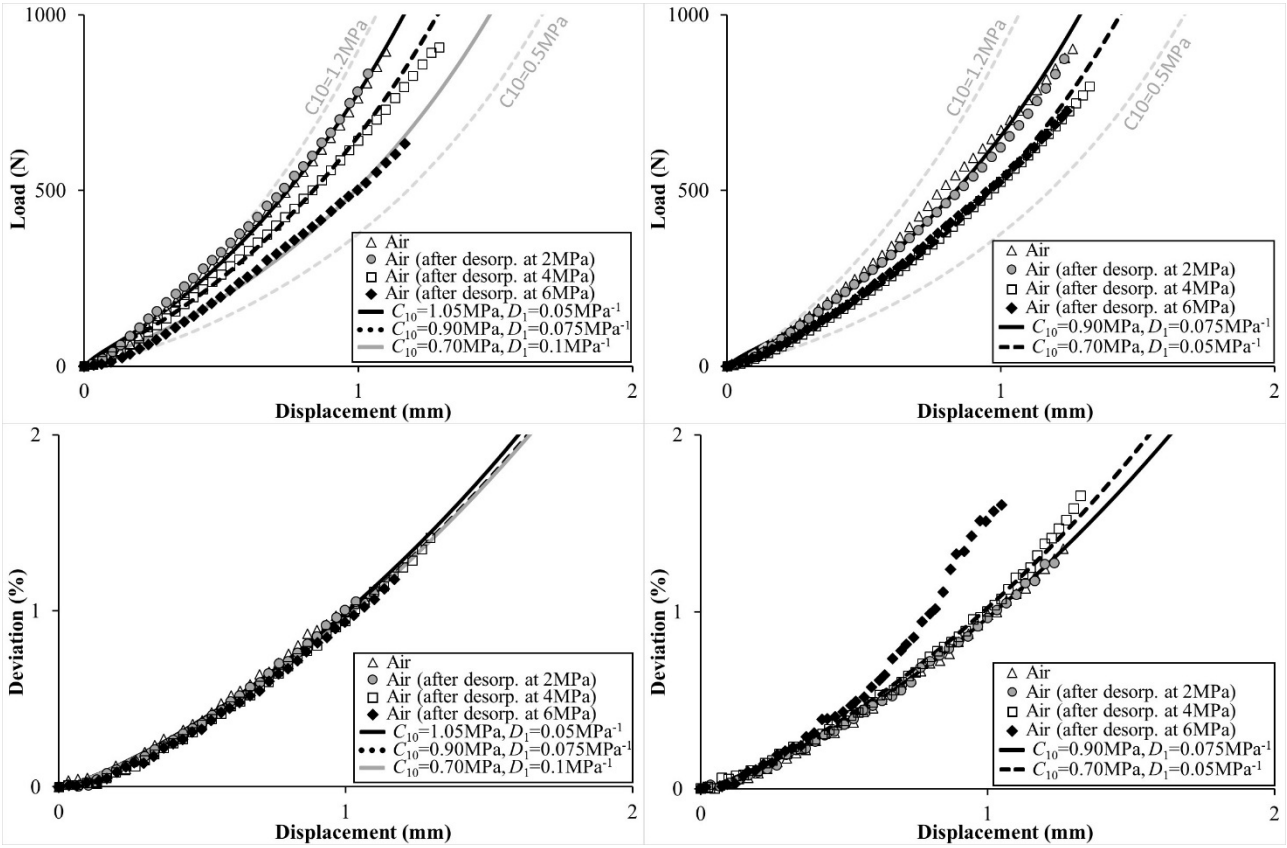

(a) (b)

Figure 18. FKM-10GE – Compression tests under air at (a) 60°C and (b) 130°C after CO_2 desorption

4.6 Observations

In order to characterize the damage in-situ during CO_2 desorption, the acquisition of the images was carried out during the decompression after the compression tests (examples: Figure 19, Figure 20, Figure 21, Figure 22, Figure 23 and Figure 24). Table 3 presents the results for each material of the damage observed during CO_2 desorption from the different conditions. By analyzing the different images, two types of damage were found which appeared in certain configurations (pressure, temperature) in the seals during CO_2 desorption.

The first type of damage is the formation of humps observed at the sample surface by internal gas inflation - the blisters (Figure 20, Figure 21, Figure 22 and Figure 23). They are no longer visible after the chamber is opened because according to the protocol there are at least 6 hours between the time of decompression and the opening of the chamber. These blisters are more or less large, for example Figure 22b shows small blisters for HNBR-10GE (60°C and 6MPa), while large local swellings are present in Figure 19b for FKM (60°C, 4MPa).Thus, after total desorption of the seal, the blisters disappear and therefore reversible. However, it is possible that one or more cracks may be present in the seal section where the blister appeared.

The second type of damage observed is at the moulding junction of the manufacturing process (parting line of the O-ring) where a seal cracking appears to occur in this area. This damage is irreversible and can be seen after the seal has been removed from the enclosure.

First, there is no visible damage to the HNBR seal. This confirms the mechanical results presented above, since whatever the sorption pressure, neither the rigidity nor the compressibility of the seal had been modified after desorption into CO_2. For the FKM seal, no damage appears at the time of desorption at 2MPa, either at 60 and 130°C. On the other hand, at 4 and 6MPa (and for both temperatures), blisters appeared during desorption (Figure 21). These may be the cause of the loss of

stiffness that was observed in these configurations during compression tests. However, it seems that this does not affect the compressibility coefficient.

Table 3. Summary for each material of the damage observed during CO_2 desorption from the different conditions.

Temperature (°C)		60			130	
CO_2 Pressure (MPa)	2	4	6	2	4	6
HNBR	No Damage					
FKM	No Damage	Blisters	Blisters	No Damage	Blisters	Blisters
HNBR-10GE		No Damage	Small Blisters		Blisters	Blisters + Cracking
FKM-10GE		Blisters	Blisters		Blisters + Cracking	Blisters + Cracking

The HNBR-10GE and FKM-10GE seals suffered extensive damage. If, as for HNBR and FKM, no damage occurred after desorption from 2MPa at 60 and 130°C, damage appeared under the other conditions. For the HNBR-10GE, blisters appeared in the following configurations: at 60°C and 130°C, 4 and 6MPa. On the other hand, at 60°C and 6MPa, only small blisters (Figure 22b) appeared during decompression. For other conditions, swelling was much more important. At 6 MPa and 130°C the HNBR-10GE seal appears to open in its parting line as shown in the Figure 23. Finally, for the FKM-10GE, blisters appeared at 60°C during the desorption of 4 and 6MPa. At 130°C for these last two pressures, blisters and a crack were present (Figure 23 and Figure 24).

It may be thought that the nature of the reinforcements and / or the process of implementation is at the origin of this weakness. It is important to note that the less intense damages correspond to more small local swelling (blister). Such damage seems to recover after a long time after desorption.

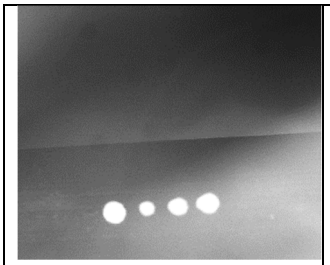

(a)

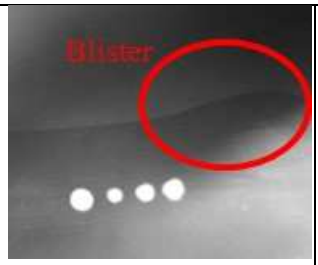

(b)

Figure 19 : FKM O-ring (after compression test, 60° and 4MPa) (a) Photo before decompression t=0s (b) Photo during decompression t=9min.

(a)

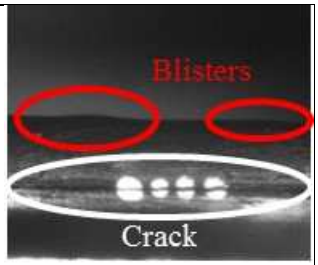

(b)

Figure 20. FKM-10GE O-ring (after compression test, 130° and 4MPa) – (a) Photo before decompression t=0s – (b) Photo during decompression t=4min.

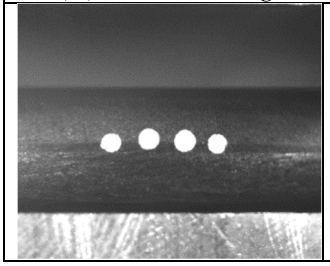

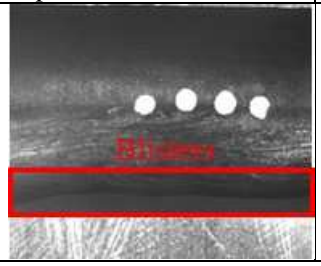

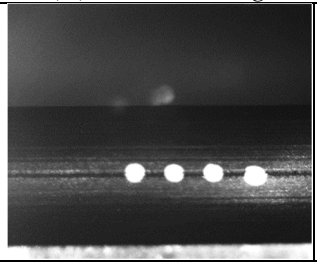

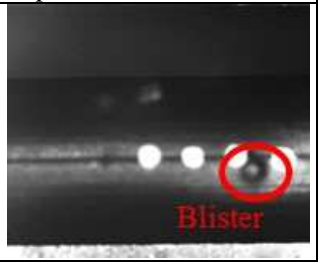

(a)	(b)	(a)	(b)
Figure 21 : FKM-10GE O-ring (after compression test, 60° and 6MPa) (a) Photo before decompression t=0s (b) Photo during decompression t=4min.		*Figure 22. HNBR-10GE O-ring (after compression test, 60° and 6MPa) – (a) Photo before decompression t=0s – (b) Photo during decompression t=5min.*	
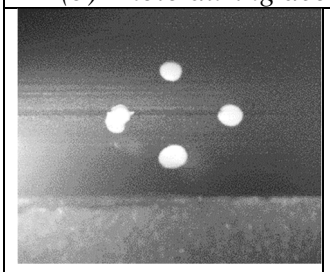	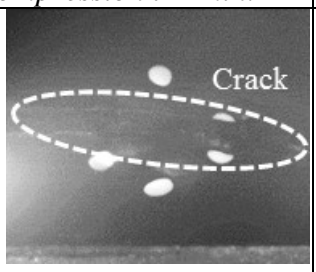		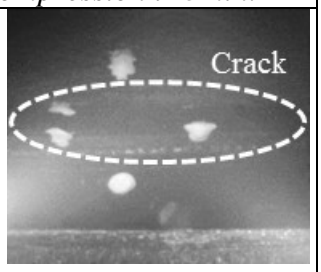
(a)	(b)	(a)	(b)
Figure 23 : HNBR-10GE O-ring [11] *(after compression test, 130° and 6MPa) (a) Photo before decompression t=0s (b) Photo during decompression t=7min.*		*Figure 24. FKM-10GE O-ring* [11] *(after compression test, 130° and 6MPa) – (a) Photo before decompression t=0s – (b) Photo during decompression t=3min.*	

4.7 Extensions

Figure 25a and Figure 25b present the values identified for each material of the coefficient C_{10} of the behavior law (equation 2) at 60 and 130°C respectively, as well as the corresponding trendlines. Figure 25 a and Figure 25b show that the coefficient C_{10} can be considered linearly dependent (trendline) on both the CO_2 pressure for HNBR, FKM and the two filled materials 10GE. If the FKM is more rigid than the HNBR in the initial state (Air), it becomes less rigid than the HNBR after the 2MPa pressure. It is therefore much more affected by CO_2 than HNBR. On the other hand, the fillers completely change the CO_2 behavior of the two initial matrices (HNBR and FKM). Figure 26 shows the effect of CO_2 pressure on the compressibility of materials. The higher the pressure is, the more the material tends towards incompressibility. Only HNBR stands out, because its compressibility does not seem to be affected at 60°C and very slightly at 130°C. For HNBR, as already mentioned, there is a low linear dependence at 130°C but none at 60°C.

The behavior law (eq. 2) can therefore be written as follows:

$$W = C_{10}[P_{CO_2}, T]\,(I_1;^{-} - 3) + D_1[P_{CO_2}, T]\,(J - 1)^2 \tag{5}$$

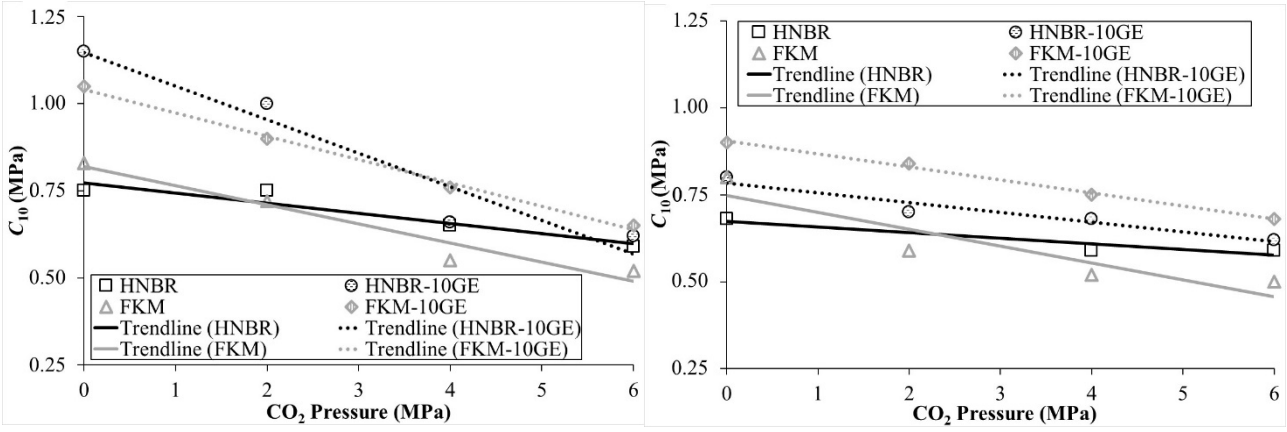

(a) (b)

Figure 25. C_{10} coefficient variation as a function of CO_2 pressure and temperature for each material- (a) 60°C, (b) 130°C

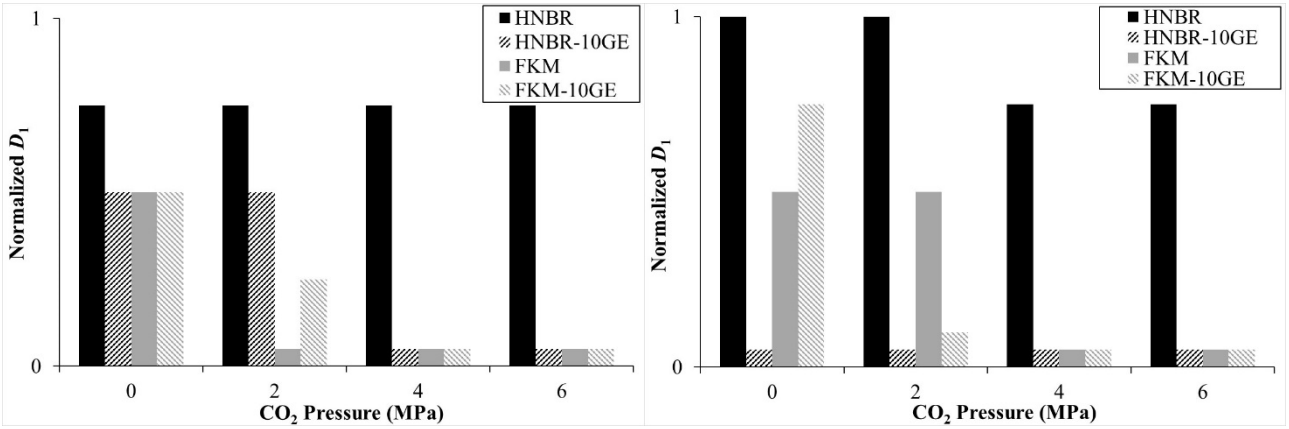

Figure 26. D_1 coefficient as a function of CO_2 pressure and temperature for each material- (a) 60°C and (b) 130°C

5 CONCLUSIONS

First of all, it should be noted that for the four materials in the study, their behavior is more or less affected by the presence of CO_2. Overall, the higher the pressure is, the lower the rigidity is, making the material more and more incompressible (because the coefficient of compressibility increases) or remains unchanged.

HNBR seems not to be affected by CO_2 under the conditions of the study. The behavior after decompression and total desorption of CO_2 is not modified, whatever the mechanical loading seen by the O-ring. Whatever the temperature (60 and 130°C), the compression behavior of the FKM seals is affected by the CO_2 pressure. Thus, as the pressure increases, the stiffness decreases. The effect of CO_2 desorption and therefore decompression on compression stiffness seems to have an effect on the FKM matrix. It was only after having had less than 6MPa of CO_2 at 60°C and 4MPa of CO_2 at 130°C that the material saw its compression rigidity slightly decrease. The compression behavior of HNBR-10GE is affected by CO_2 only at 60°C. At the second temperature (130°C), as for HNBR, there is no effect of pressure on the behavior. On the other hand, after desorption, there is a non-negligible loss of rigidity above 4MPa at 60°C and 2MPa at 130°C. The material appears to have been damaged either by the CO_2 pressure or during decompression.

The behavior of the FKM-10GE is affected by CO_2 in compression (loss of rigidity). Thus, the effect of the pressure under 2MPa of CO_2 and the decompression lead to damage to the FKM-10GE which results in a loss of compression stiffness after return at zero pressure. This FKM-10GE material appears to associate the weaknesses of the FKM matrix with those induced by the 10GE reinforcements in a matrix. Finally, among the four materials studied in these temperature and CO_2 pressure ranges, HBNR is the most suitable material for these critical environments (temperature, CO_2 pressure). Although the materials are different, these results support those obtained by Davies et al [7] on other elastomers, on the critical condition of 4MPa.

It is easy to highlight the effect of the matrix on one hand and the effect of the reinforcements on the other hand. Thus, it can be concluded that these reinforcements have an adverse effect on behavior. In the end, from a certain pressure there is a modification of the behavior of the materials, which should be studied further in order to firstly better understand mechanisms then to be able to translate them from a point of view behavior law. But the pressure criteria does not applied because the breaks are delayed, there is no longer any external mechanical pressure and the diffusion has already acted, so that the prediction of the rupture in this framework of gaseous conditions under temperature is an open issue.

6 ACKNOWLEDGEMENTS

This work was financially supported by the French CPER and European FEDER.

7 REFERENCE

[1] B. Alcock, T.A. Peters, R.H. Gaarder, J.K. Jørgensen, The effect of hydrocarbon ageing on the mechanical properties, apparent crosslink density and CO_2 diffusion of a hydrogenated nitrile butadiene rubber (HNBR) , Polym. Test. 47 (2015) 22-29.

[2] T. Grelle, D. Wolff, M. Jaunich, Temperature-dependent leak tightness of elastomer seals after partial and rapid release of compression, Polym. Test. 48 (2015) 44-49.

[3] S.Z. Qamar, & M.Akhtar, & T. Pervez, & M.S.M. Al-Kharusi, Mechanical and structural behavior of a swelling elastomer under compressive loading, Materials and Design, 45 (2013) 487-496.

[4] B.J. Briscoe, T. Savvas, C.T. Kelly, Explosive decompression failure of rubbers - A review of the origins of pneumatic stress-induced rupture in elastomers, Rubber Chem. Technol. 67 (3) (1994) 384–416.

[5] B.J. Briscoe, C.T. Kelly, The effect of structure on gas solubility and gas induced dilation in a series of poly(urethane) elastomers, Polymer 37 (5) (1996) 3405-3410.

[6] Z Major, R.W. Lang, Characterization of the fracture behavior of NBR and FKM grade elastomers for oilfield applications, Engineering Failure Analysis 17 (3) (2010) 701-711.

[7] O.M. Davies, J.C. Arnold, S.Sulley, The mechanical properties of elastomers in high-pressure CO_2, J. Mat. Sci. 34 (2) (1999) 417-422.

[8] L. Haroonabadi, A. Dashti, M. Najipour, Investigation of the effect of thermal aging on rapid gas decompression (RGD) resistance of nitrile rubber, Polym. Test. 67 (2018) 37-45.

[9] X. Chen, H. A Salem, R. Zonoz, CO2 Solubility and diffusivity and rapid gas decompression resistance of elastomers containing CNT, Rubber Chem. Technol. 90 (3) (2017) 562–574.

[10] F. Daou, C. R. de Miranda, J. L. de Oliveira, B. Engelke, C. Borman, S. Le Roy-Delage, B. Lungwitz, Swelling of Elastomers in CO2 Environment: Testing Methodology and Experimental Data, SPE Latin America and Caribbean Petroleum Engineering Conference, 21-23 May, Maracaibo, Venezuela (2014).

[11] E. Lainé, J.C. Grandidier, G. Benoit, F. Destaing, B. Omnès, Mechanical characterization under CO2 of HNBR and FKM grade elastomers for oilfield applications – effects of 10GE reinforcements, Constitutive Models for Rubber X, Lion & Johlitz Eds, Talyor & Francis Group London (2017) 231-236.

[12] Evaluating Elastomeric Materials in Carbon Dioxide Decompression Environments, Nace Standard TM0192-98, 1998.

[13] Qualification of non-metallic sealing materials and manufacturers, Norsok Standard M-710 rev. 2, 2001.

[14] Z. Sun, G. Benoit, C. Moriconi, F. Hamon, D. Halm, F. Hamon, G. Hénaff, Fatigue crack propagation under gaseous hydrogen in a precipitation-hardened martensitic stainless steel, Int. J. Hydrogen Energy 36 (14) (2011) 8641-8644.

[15] S. Castagnet, J.C. Grandidier, M. Comyn, G. Benoit, Mechanical testing of polymers into pressurized hydrogen: tension, creep and ductile fracture, Exp. Mech. 52 (3) (2012) 229-239.

[16] Abaqus/CAE User's Guide. Ver. 6.13, Vol.3, Dassault Systèmes Simulia Corp., Providence, RI, USA (2013).

[17] L.R.G. Treloar, The physics of rubber elasticity, Oxford University Press, 1975.

[18] O.H. Yeoh, Developments in Finite Element Analysis, Engineering with Rubber, Carl Hanser Verlag GmbH & Co. KG (2012) 345-364.